Research Article

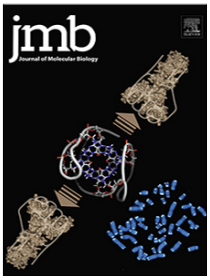

Modulating Microtubules: A Molecular Perspective on the Effects of Tail Modifications

Lavi S. Bigman and Yaakov Levy *

Department of Chemical and Structural Biology, *Weizmann Institute of Science, Rehovot 76100, Israel*

Correspondence to Yaakov Levy: *Koby.Levy@weizmann.ac.il (Y. Levy)*
https://doi.org/10.1016/j.jmb.2021.166988
Edited by Richard W. Kriwacki

Abstract

Microtubules (MTs), an essential component of the eukaryotic cytoskeleton, are a lattice of polymerized tubulin dimers and are crucial for various cellular processes. The genetic and chemical diversity of tubulin and their disordered tails gives rise to a "tubulin code". The functional role of tubulin post-translational modifications (PTMs), which contribute to the chemical diversity of the tubulin code, is gradually being unraveled. However, variation in the length and spatial organization of tubulin poly-modifications leads to an enormous combinatorial PTM space, which is difficult to study experimentally. Hence, the impact of the combinatorial tubulin PTM space on the biophysical properties of tubulin tails and their interactions with other proteins remains elusive. Here, we combine all-atom and coarse-grained molecular dynamics simulations to elucidate the biophysical implications of the large combinatorial tubulin PTM space in the context of an MT lattice. We find that tail–body interactions are more dominant in the tubulin dimer than in an MT lattice, and are more significant for the tails of α compared with β tubulin. In addition, polyglutamylation, but not polyglycylation, expands the dimensions of the tubulin tails. Polyglutamylation also leads to a decrease in the diffusion rate of MT-associated protein EB1 on MTs, while polyglycylation often increases diffusion rate. These observations are generally not sensitive to the organization of the polymodifications. The effect of PTMs on MT charge density and tail dynamics are also discussed. Overall, this study presents a molecular quantification of the biophysical properties of tubulin tails and their polymodifications, and provides predictions on the functional importance of tubulin PTMs.

Introduction

Microtubules (MTs) are an essential component of the eukaryotic cytoskeleton and play an important role in cell division, provide mechanical support to the cell, and serve as "highways" for intracellular trafficking. The basic building block of MTs (Figure 1(A) and (B)) is the tubulin heterodimer, which is composed of α and β tubulin units, with the units in turn composed of a folded globular part (the "body") and a disordered electronegative tail (Figure 1(C)). The tubulin heterodimers polymerize to form elongated hollow cylinders, usually composed of 13 protofilaments that associate laterally to form a closed tube (Figure 1(A)).[1,2]

The amino-acid sequence of the tubulin body is highly conserved (80–95% sequence identity), however tubulin tails exhibit a significant degree of sequence variation between isoforms (~50% identity)[3] and are targets for many post-translational modifications (PTMs), including polyglutamylation, polyglycylation and de-tyrosination. Additional PTMs (e.g. phosphorylation, acetylation and polyamination) may occur on the tubulin body.[4–6] The combined genetic and chemical diversity of tubulin is often referred to as "the tubulin code". In humans, eight isoforms of α and ten

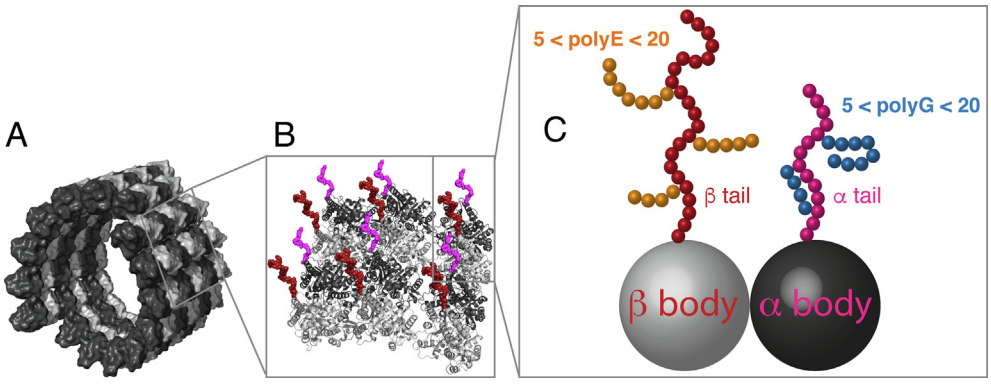

Figure 1. Structure of microtubules and their post-translational modifications. (A) Side view of a slice of a microtubule composed of repeating units of α and β tubulin, shown in dark and light gray, respectively. (B) Zoom in on a portion of the microtubule showing a 3 × 2 lattice of tubulin heterodimers comprised of a 3 × 4 lattice of monomeric α and β tubulin proteins, showing the disordered tails of α (magenta) and β tubulin (red). A 3 × 4 lattice was used in this work to study the biophysical properties of tubulin tails and their modifications in the context of a microtubule lattice. (C). Zoom in on a tubulin dimer. The folded tubulin "body" is shown as spheres, and the disordered C-terminal tails as elongated chains. In our model, the tail on the β tubulin (labelled as the β tail; 24 residues) is longer than the tail on the α tubulin (labelled as the α tail; 14 residues). Polyglutamylation and polyglycylation can occur on the tails of both α and β, with the figure showing a polyglutamate substituent chain on the tail of the β tubulin subunit and a polyglycine substituent chain on the tail of α tubulin subunit solely for reasons of clarity. In this study, we vary the length of the substituted polyglutamylate (orange) and polyglycine (blue) chains from 5–20 residues, and also examine different tethering positions for the tail modifications. Note that the polyglycine substituent chains are shown as having a compact configuration whereas the polyglutamate substituent chains are shown as more expanded on the basis of data presented in Figure 3.

isoforms of β tubulin have been identified. In this study, we focus on polyglutamylation and polyglycylation, two PTMs found mostly on tubulin tails, and hence are likely to have evolved to impact tubulin tail function, as several reports suggest (Figure 1 (C)).[6–8]

Tubulin tails regulate MT functions and interactions with other proteins, including the motor proteins kinesin and dynein and several intrinsically disordered proteins, such as Tau and MAP2.[9,10] In addition, accumulating evidence suggests that tubulin tail modifications provide an additional layer of regulation to MT function.[6–8] For example, polyglutamylation, a common modification in neuronal and axonemal MTs, was shown to regulate the processivity of several motor proteins[11] and the activity of the MT severing enzymes spastin and katanin.[12–14] In addition, polyglutamylation leads to a decrease in the diffusion rate of proteins on MTs[15] which is a common and functionally important protein transportation mode on MTs.[16,17] An excess of polyglutamylation was also shown to perturb neuronal transport.[18] Polyglycylation is another common modification, found mostly in axonemal MTs. The functional role of polyglycylation is still not fully understood, however it was shown that polyglycylation is important for maintaining the stability of axonemal MTs[19] and that the persistence length of polyglycylated MTs is lower than that of polyglutamylated MTs, indicating that polyglycylation leads to a decrease in MT stiffness.[20] A recent study showed that tubulin glycylation controls axonemal dynein activity, flagellar beat, and affects male fertility.[21] Importantly, several links between mis-regulation of tubulin PTMs and human disease have been documented.[6,22]

Deciphering the functional role of tubulin PTMs is rendered even more complex because different lengths and spatial organizations of poly-modification are possible, thus giving rise to an enormous combinatorial PTM space. For example, neuronal tubulin can bear polyglutamate chain substituents of length up to 11 glutamates[23] and axonemal tubulin can bear up to 21[24] glutamates and 40 glycines.[25,26] These modifications can be initiated, in principle, from any glutamic acid in the tail. Moreover, specific classes of modification enzymes are dedicated to either the initiation or elongation of poly-modifications[27–29] which gives rise to the possibility that specific lengths and spatial organizations of PTMs perform distinct functional and regulatory roles.

Several studies have investigated the dynamics of tubulin tails as isolated peptides, or in the context of a tubulin dimer. Computational studies suggest that the tails of α and β tubulin interact with distinct binding sites on the bodies of both α and β tubulin.[30,31] The computational results are consistent with NMR data,[26] which show that β-tubulin tails in the context of a tubulin dimer exhibit a chemical shift in comparison with the β-tail as an isolated peptide, indicating that they interact with the tubulin body. Moreover, different degrees of polyglycylation were found to affect (to some

extent) the conformational ensemble of the tubulin tail.[26] However, since tubulin dimers usually function in the context of an MT lattice, under some conditions tubulin tails may behave not as conventional tethered chains characterized as intrinsically disordered regions (IDRs), but rather as molecular polymer brushes characterized by strong inter-chain interactions that significantly alter the surface-related properties of the lattice and its functionalities.

Due to the functional importance and the critical regulatory role of tubulin tails and their modifications, it is likely that the intrinsic properties of the tails, such as their flexibility, dimensions, conformational dynamics and interactions with the tubulin body, will contribute to their functional and regulatory roles. However, a detailed quantification of the biophysical properties of tubulin tails and their modifications at the molecular level remains elusive. Since tubulin dimers usually function in the context of an MT, it is important that such quantification also be undertaken in a lattice context.

Here, we use a combination of all-atom and coarse-grained (CG) molecular dynamics (MD) simulations to quantify, with atomistic or near atomistic precision, how various degrees of polyglutamylation and polyglycylation (Figure 1(C)) affect the structure, function, dynamics, and interactions of tubulin tails in the context of an MT lattice (Figure 1(B)). This is achieved by studying MT variants bearing polyglutamate or polyglycine chain substituents of varying length and connected to the tubulin tail at different points. In addition, in order to examine the functional impact of the various modifications, we used CG-MD to quantify the diffusion rate of the EB1 protein, which is involved in the regulation of MT length, on modified MTs.

Our results show that tail–body interactions are more dominant in the tubulin dimer than in the context of an MT lattice, and that they are clustered at the α/β interface. In addition, while polyglutamylation leads to a significant expansion in the dimensions of the tubulin tails, polyglycylation does not affect tail dimensions, because polyglycine hydrophobically collapses onto itself and onto the tubulin tail. Moreover, while polyglutamylation leads to a decrease in the diffusion rate of EB1 on MT, polyglycylation often increases the diffusion rate. These observations only mildly depend on the spatial organization of the poly-modifications. Notably, our results are not force-field dependent. Hence, our results provide a detailed biophysical quantification of the dynamics and interactions of tubulin tails and their modifications in the context of the MT lattice. They explain the underlying mechanism behind experimentally determined functions of tubulin PTMs, and provide predictions as to how tubulin modifications affect MT stability, function, and interactions with other proteins.

Results

Model generation

We sought to quantify the biophysical properties of tubulin tails and their modifications, while considering possible interactions between tails and bodies, between adjacent tails, and between substituent chains and the tail to which they are bound, all in the context of an MT lattice. We therefore constructed an atomistic model of a 3×4 MT lattice (Figure 1(B), See *Methods* for details); thus, the central α/β tubulin dimer was surrounded by additional tubulin monomers. In the model, the lateral distance between tails was $\sim$ 5 nm and the longitudinal distance was $\sim$ 4 nm. These distances are similar to the $\sim$ 5 nm fully extended lengths of the tails of α tubulin (5 nm, 14 amino acids) and β tubulin (9 nm, 24 amino acids). However, considering the $\nu = 0.6$ Flory scaling exponent for disordered polymers, the expected actual mean radius of gyration (Rg) was $\sim$ 1.7 nm and 2.5 nm for α and β tubulin, respectively, which is much smaller than the distance between their anchoring points and, consequently, significant interactions were not expected between tubulin tails. When long polyglutamate chain substituents are added to the original tails of MT, electrostatic repulsions are likely to influence the biophysical properties of tubulin tails and their dimensions. Hence, using a 3×4 lattice, we can explore the properties of tubulin tails from the perspective of a polymer brush, and quantify the effects of neighboring tubulin subunits on each other's tails.

The tubulin tails were modeled as elongated chains, and more realistic conformations were achieved during the simulations (see *Methods*). Polyglutamate (Figure 1(C), orange) and polyglycine (Figure 1(C), blue) chain substituents of length of 5–20 residues were connected by a peptide bond to glutamate residues on the original tubulin tail (see *Methods* for details). Whereas the MT body remained static in our simulations, the tails and their modifications were flexible. The conformational dynamics of tubulin tails and their modifications were simulated using unbiased atomistic or CG molecular dynamics simulations.

Tail–body interactions: Dimeric tubulin versus MT lattice

First, we examined, using all-atom simulations, the interactions between α and β tubulin tails and the tubulin bodies that make up the MT lattice, and tested to what extent tubulin tails project from of the MT surface for WT tubulin and the

poly-modified variants. The interaction energy between α and β tubulin tails and the residues of the tubulin bodies in the MT lattice is negative, indicating that tail residues interact with body residues in MT lattices comprised of WT tubulin (Figure 2(A) and (B), black line), polyglutamylated tubulin (Figure 2(A) and (B), orange line), and polyglycylated tubulin (Figure 2(A) and (B), cyan line). Interestingly, the interaction energy between tail and body is stronger for the α tail compared with the β tail, consistently with a recent NMR study.[20] To test whether the extent of tail–body interactions depend on the tubulin dimer being situated in an MT lattice, we preformed additional all-atom simulations of an isolated WT tubulin dimer. We found that the tail–body interaction energy was lower in the dimer compared with the lattice, being ~ 2-fold lower for α tubulin tails and ~ 4-fold lower for β tubulin tails (Figure 2(A) and (B), dashed line). Several studies[20,30,31] relied on tubulin dimers to report on tail–body interactions, however our findings suggest that the presence, precise identity, and duration of tail–body interactions differ in a dimer compared with an MT lattice.

A distance-matrix analysis conducted between tail residues and the charged body residues reveals that most interactions involve tail residues that are very close to the tail anchoring point (namely, α 438 and β 427), and that an additional interaction involves residue E431 in β tails and residue E441 in α tail. The β tail interacts with residues 400–402 of the α body closest to it, whereas the α tail interacts with residues 390–392 of the β body closest to it (Figure S1). We did not observe any cross-protofilament interactions. We also tested whether polyglutamylation or polyglycylation of the tails affect the specific interactions between α E441 or β E431 tail residues and the tubulin body (tail-body interactions involving these residues have been previously reported[30,31]). Although the distance distribution between β E431 and α K401 is similar for WT and polyglutamylated or polyglycylated tails (Figure 2(D), selected conformation shown in panel

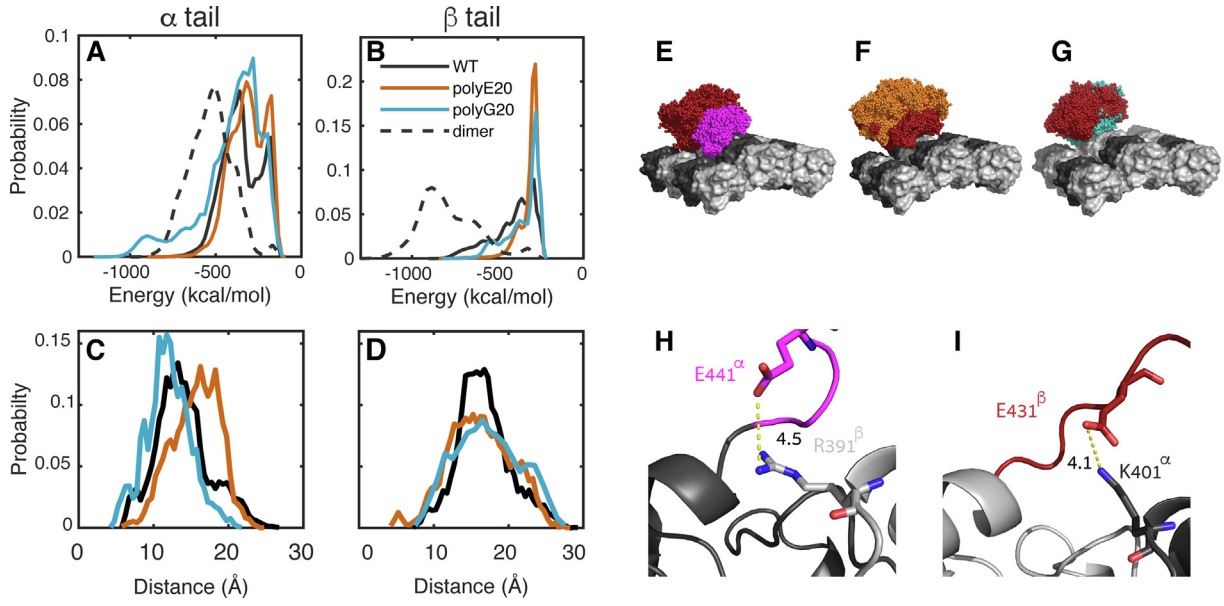

Figure 2. Tubulin tail–body interactions. (A–B) Interaction energy between the residues of the body and the tail for the case of an α/β dimer (dotted black line) and three types of 3 × 4 MT lattice, with (A) showing interactions involving the tail of α tubulin and (B) showing interactions involving the tail of β tubulin. The lattices were composed of wild-type (WT) tubulin α/β dimers (solid black line) or of α/β polyE20-tubulin (orange) or polyG20-tubulin (cyan) dimers (*i.e.,* dimers in which the tails on the α/β tubulins were substituted with 20-residue polyglutamate or polyglycine chains, respectively). Note that the tail–body interaction energy is lower in the dimer case compared with the lattice cases. (C–D) Distribution of the distances between the Cα atoms of (C) residue E441 (on the tail of α tubulin) and residue R391 (on the body of β tubulin) and (D) residue E431 (on the tail of β tubulin) and residue K401 (on the body of α tubulin) for lattices constructed from WT-tubulin (black), polyE20-tubulin (orange), and polyG20-tubulin (cyan). (E–G) Overlay of tail conformations of α tubulin (magenta) and β tubulin (red) from 10 independent 100-ns atomistic simulations per lattice of (E) WT-tubulin, (F) α/β polyE20-tubulin (glutamate chain residues in orange), or (G) α/β polyG20-tubulin (glycine chain residues in cyan). For clarity, we show only the conformations of the tails of the central α/β tubulin dimer (panel E) or β tubulin (panels F-G). (H-I) Snapshots demonstrating the interaction between residue pairs shown in panels C-D, respectively. The distances between the interacting residue pairs are shown on the figure in black, and are in Å.

I), the distance between α E441 and β R391 is sensitive to modifications: polyglutamylation leads to an increase in the tail–body distance (Figure 2(C), orange, selected conformation shown panel H) and polyglycylation leads to a decrease in the tail body distance (Figure 2(C), cyan). This implies that modifications of α tails, but not of β tails, can regulate tail–body interactions in tubulin.

In Figure 2(E), we show an overlay of 10 independent MD simulation runs, each 100 ns long, of the conformational space covered by α (magenta) and β (red) WT tails. The "mushroom" shape of both conformational spaces demonstrates that tail–body interactions are localized and transient. In Figure 2(F) and 2G, we show the conformations for variant tubulins. The specific variant is denoted by the type of modification (where polyE represents polyglutamylation and polyG represents polyglycylation) and refers to the number of glutamate or glycine residues in the substituent, thus, polyE5-tubulin and polyG10-tubulin indicate tubulin variants whose tails were substituted with a 5-residue chain of glutamates or a 10-residue chain of glycines, respectively. Figure 2(F) shows an MT lattice comprised of polyE20-tubulin with modified β tails. The "mushroom" shape is preserved, and the residues comprising the polyglutamate chain substituent (orange) are clearly distanced from the tail residues, and do not interact with the body. A different conformational space is created when the β tails are polyglycylated (Figure 2(G)): in the polyG20-tubulin variant, the mushroom shape is preserved, but the residues of the glycine chain substituent (cyan) are positioned closer to the tubulin bodies of the MT lattice.

These results give rise to a plausible mechanism in which α and β tubulin tails play distinct functional regulatory roles. The principal role of β tubulin tails is to regulate interactions with other proteins (as evidenced by MT-severing enzymes[12,32] and by their role in the diffusion of protein on MTs),[15] whereas the α tails regulate tail–body interactions, and thus regulate the mechanical stability of MTs.[20]

Dimension of the tail: Polyglutamylation expands whereas polyglycylation collapses the tails

Having quantified tail–body interactions, we sought to quantify the biophysical properties of the tubulin tails themselves. Hence, we studied, at atomistic precision, the dynamics of MT lattices comprised of WT tubulin, and tubulin whose tails were modified to bear polyglutamate or polyglycine chains comprised of 5, 10, 15, or 20 residues (denoted as polyG5–polyG20 and polyE5–polyE20 substituent chains), resulting in a total of nine variants. We found that the addition of polyglycine chains has little effect on the radius of gyration (Rg) of tubulin tails (Figure 3(A)). By contrast, the addition of polyglutamate chains leads to a gradual, monotonic increase in the Rg of both α and β tubulin tails (Figure 3(B)). The difference in dimensions between polyglycylated and polyglutamylated tubulin tails in the context of an MT lattice is also clear from looking at selected conformations of the modified tails (Figure 3(C)–(F)). We note that polyglycylated tails sample various collapsed conformational forms in which the residues of the substituted chain interact either with themselves, or with the tubulin tail backbone.

Polymeric properties of tubulin modifications

To further quantify the molecular origin of the collapse of polyglycylated tails and expansion of polyglutamylated tails, we calculated the distance between every combination of residues i and j on α and β polyE20-tails and polyG20-tails. The results are summarized as distance matrices (Figure 4(A) and (B)). For both α and β polyG20-tails, there is a clearly-defined area characterized by dark shades of gray situated below and to the left of the diagonal, indicating distances of < 10 Å between residue j of the substituent chain and the residues of the tail (marked with a cyan rectangle). In addition, there are dark shades of gray on the lower right-hand side near the diagonal in Figure 4 (A) and (B), indicating that the polyG20 residues are also located in close proximity to each other. This pattern is not observed for polyE20-tails, as can be seen by the light shades of gray in the orange rectangles (upper diagonal in Figure 4(A) and (B)). Hence, we conclude that the collapse of polyglycylated tails has two origins: substituent chain–chain self-interactions and interactions between the residues of the substituent chain and the tail to which it is attached.

The difference between the polyglycine and polyglutamate substituent chains is also apparent when looking at their polymeric properties. According to Flory,[33] the Rg of a polymer scales with the number of bonds in the polymer (N) and an exponent ν, $Rg \propto N^{\nu}$. Due to the fractal nature of proteins in a good solvent, a similar relation can be obtained by calculating Rg as a function of the inter-residue distance in a single chain.[34] Hence, we use $Rg \propto |i-j|^{\nu}$, where | *i-j* | is the sequence separation between two residues in the substituent chain tail. Polymer theory predicts a scaling of ν = 1/3 for a polymer in poor solvent, ν = 0.5 for a polymer in a theta solvent, and ν = 3/5 for a polymer in a good solvent. Whereas folded proteins scale with ν = 1/3, many IDPs scale with ν = 2/3, resembling a polymer in good solvent.[35]

We used this relation to derive the Flory exponents ν for the polyglycine and polyglutamate substituent chains (the residues comprising the tail were not included in this calculation). We found ν (polyG) ~ 0.6–0.7 (Fig4(C) and (D), cyan) and ν (polyE) ~ 0.9 (Figure 4(C) and (D), orange). The value for the polyglycine substituent chain is very

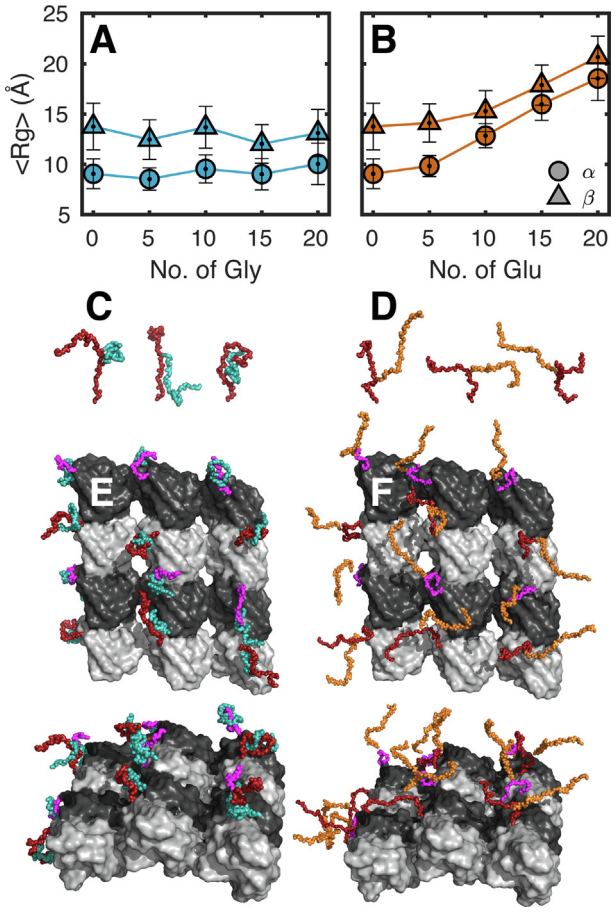

Figure 3. Polyglutamylated tails are expanded but polyglycylated tails are collapsed. (A) The radii of gyration (Rg) of (A) polyglycylated and (B) polyglutamylated tubulin tails as a function of the number of residues in the substituent chain. Rg was calculated separately for the tails of α (circles) and β (triangles) tubulin subunits from all-atom MD simulations of 3 × 4 lattices of wild-type (WT) tubulin (0-residue chain) and variants with modified tails bearing substituent chains of length 5, 10, 15, or 20 residues. In each case, the Rg was obtained by averaging at least seven 100-ns simulations of each construct. Note that whereas the Rg of polyglycylated tails is similar to that of unmodified tail, the Rg of polyglutamylated tails increases monotonically with the length of the modification for both α and β tubulin. (C–D) Selected conformations of β tubulin tails (C) polyglycylated with a 20-residue chain (polyG20-tail) or (D) polyglutamylated with a 20-residue chain (polyE20-tail). The presented conformations were selected from a tubulin at the center of the simulated microtubule lattice. Note that in all configurations, the polyG20-substituent is collapsed either onto itself or onto the tail whereas all polyE20-tail samples exhibit expanded configurations. (E-F) Selected conformations of polyG20-tubulin (panel E) and polyE20-tubulin (panel F) systems, showing the whole 3 × 4 lattice used in this study.

close to the expected ν = 3/5 for an IDP, as polymers in good solvent. Earlier studies[36] on isolated polyglycine chains in water support their compact conformation with Flory exponent that is even lower than 3/5. We attribute the difference to the fact that in the case of modified tubulin tails, the polyglycine chains are tethered to an otherwise unmodified tubulin tail, and hence can interact both with neighboring residues on the tubulin tail and with other residues in the substituent chain. The values of the Flory exponent for polyglutamate substituent chains are close to 1, as expected for a highly charged polyelectrolyte chain.[37,38]

Interestingly, WT tubulin tails have an intermediate Flory exponent value of ν ~ 0.85, which is also expected, due to the charge densities of the polymer chains, which are −0.57 and −0.45 for α and β tubulin, respectively. The addition of polyglutamate or polyglycine substituent chains does not affect the Flory exponent for the WT tail residues (empty bars in Figure 4(D)).

Impact of the spatial distribution of polymodifications on the structure, function, and dynamics of tubulin tails

Having elucidated the effect of different lengths of polyglutamate or polyglycine substituent chains on the biophysical properties of tubulin tails, we

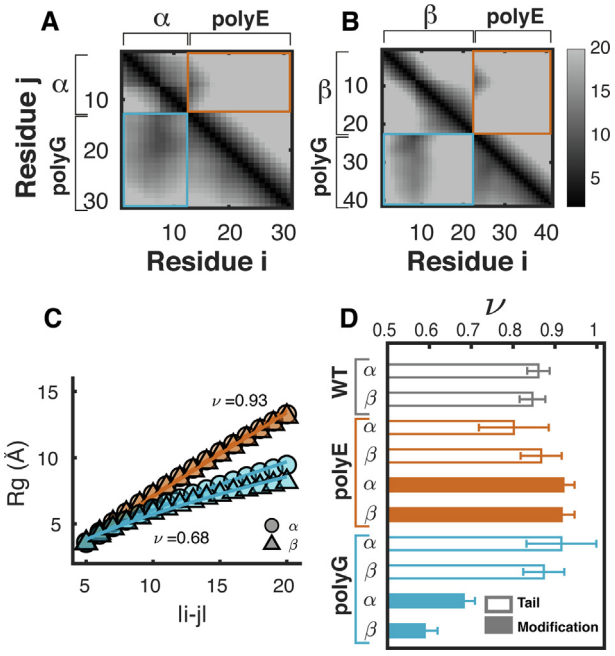

Figure 4. Scaling behavior of tubulin modifications. (A–B) Matrices of the average distances (in Å; as per gray-scale bar on right) between residues *i* and *j* in the tails for (A) the α tubulin subunit and (B) the β tubulin subunit of polyG20-tubulin (lower diagonal triangle) versus polyE20-tubulin (upper diagonal triangle). The *i–j* distances are often < 10 Å for the polyG20-tubulin system (marked in a cyan rectangle), but > 20 Å for the polyE20-tubulin system (as indicated by the orange box). In addition, the substituent chain–chain distances are < 10 Å in the case of polyG20-tails, but not polyE20-tails, as can be seen in the right-hand side of the lower diagonal. (C) Rg as a function of the inter-residue sequence separation |i-j|, for the substituent chain residues only for the tails of α (circles) and β (triangles) polyE20-tubulin (orange) and polyG20-tubulin (cyan) (*i.e.*, only the residues of the modifications and not of the tails are considered in these calculations). The line shows the fit of the data to the Flory scaling expression: Rg ~|i-j|ν. (D) Flory's scaling exponent ν is shown for the α and β tubulin tails on unmodified tubulin (empty gray bars), the wild-type tail residues (empty orange bars) and substituent chain residues of polyE20-tubulin (filled orange bars), and wild-type tail residues (empty cyan bars) and substituent chain residues (filled cyan bars) of polyG20-tubulin. The value of ν for the unmodified residues is ν ~ 0.8, for the polyE20 substituent chain residues is ν ~ 0.9, and for polyG20 substituent chain residues is ν ~ 0.6–0.7. Error bars correspond to the standard deviation of ν calculated from 10 independent 100-ns atomistic molecular dynamics runs.

sought to examine how the tethering position and distribution of poly-modifications affect tail properties. For that purpose, we constructed a CG model of an MT modelled as a 3 × 4 lattice of tubulin monomers in which each amino acid is represented by a single bead in the position of the Cα atom (see *Methods*). Electrostatic interactions were included in our model using the Debye-Hückel potential, and hydrophobic interactions were included using the hydrophobicity scale (HPS) model[39] (*Methods*). We calibrated our CG model against the atomistic data for tubulins substituted with polyE5–polyE20 and polyG5–polyG20 chains, (Figure S2-3) to assign the salt concentration and strength of hydrophobic interactions that result in a tubulin tail Rg in the CG model that matches the Rg from atomistic simulations.

To understand how the tethering position of a polyglutamate or polyglycine substituent chain affects tail properties, we selected three additional substituent anchoring sites on both the α and β tails. Experimental studies have shown that all four paired (α, β) anchoring locations, termed here sites 1–4, can be modified.[40–44] These four sites were substituted with either polyglutamate or polyglycine chains of different lengths. First, we constructed four variants in which polyE20 or polyG20 chains were attached to the tubulin tail at sites 1–4 (Figure 5. Top row). Second, to examine the impact of the spatial organization of modifications, we constructed three additional variants in which the polyE20 and polyG20 chains were split into two 10-residue chains that were attached at sites 1 and 2, 2 and 3, or 3 and 4 (Figure 5, middle row). Finally, we constructed a variant in which the 20 modification residues were split into four 5-residue chains that occupied all the anchoring sites we examined (Figure 5, bottom row). We performed an extensive biophysical quantification of MT lattices comprised of each of these variants, presented in Figure 6. All the values shown in Figure 6 are normalized to the WT lattices.

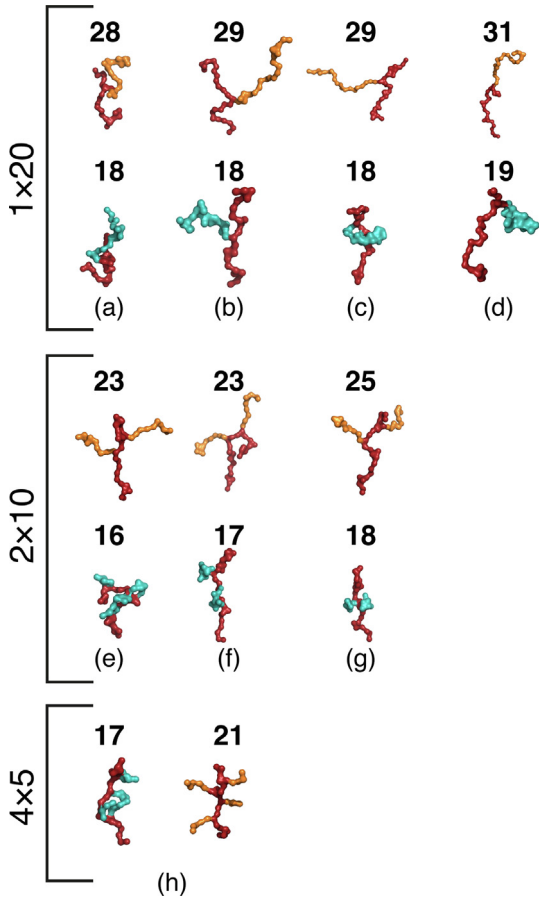

Figure 5. Representative conformations of variants with poly-modified tails. All the tails were modified to bear a total of either 20 Glu or 20 Gly residues organized as a single chain of 20 residues (a–d, top row), two chains of 10 residues each (e–g, middle row), or four chains of five residues each (h, bottom row). The selected conformations are presented in pairs for β tails (red) bearing polyglutamate (orange, upper member of pair) or polyglycine (cyan, lower member of pair) substituent chains. The modifications were attached at four selected sites. The number above each conformation is the average Rg (in Å) from 10 independent coarse-grained molecular dynamics simulations.

The first question we asked was how the tethering position and spatial organization of the modifications affect the functioning of MTs as "highways" for intracellular trafficking. Since the diffusional motility of MT-binding proteins on MTs is a common transport mode with important biological implications,[16,17,45–48] we tested how the spatial organization of modifications affects the diffusion rate of EB1 across (D_x) and along (D_y) MTs. Our main observation is that polyglutamylation of the tails of α and β tubulin leads to a decrease in the diffusion rate both across and along protofilaments (D_x, Figure 6(A) and D_y, Figure 6(B), top row of the blue panel), as can be seen by the lighter blue shades for substituted tails (the MT lattices labelled 5–20) compared with WT tails. Note, that longer polyglutamate substituent chains (consisting of 15 or 20 residues) produce slower diffusion than do shorter chains (consisting of 5 or 10 residues), but the anchoring site (MT lattices a–d) and spatial organization (MT lattices e–h) of the polyglutamate substituent chain do not significantly change the degree of decrease in the diffusion rate of EB1, as shown by a comparison of the shading in Figure 6(A) and (B) of MT lattice 20 compared with a–h. By contrast, the diffusion rate of EB1 on polyglycine MTs is often higher than its rate on WT MT, both across and along protofilaments (D_x, Figure 6(A) and D_y, Figure 6(B), lower row of the blue panel). However, although most polyglycylation systems exhibit a diffusion rate greater than that found for WT, no clear trend is observed. These observations are similar to those we found in a previous study, in which we examined the effect of modification length on protein diffusion on MTs,[15] without examining the effect of the spatial organization of the modifications.

The next quantity we analyzed was the Rg of the tubulin tails of the MT lattices. Polyglutamylation leads to an increase in Rg for the tails of both α and β tubulin (Figure 6(A) and (B), top row of green panel), with the increase proportional to the degree of modification, as we found in our atomistic simulations (Figure 3(B)). When 20 glutamates are tethered as a single chain to a tubulin tail, Rg increases ~ 2 fold relative to WT tails, independently of tethering position (MT lattices a–d in Figure 6(A) and (B)). When the 20 glutamates are split between two anchoring sites (MT lattices e–g of Figure 6(A) and (B)) or four anchoring sites (MT lattice h of Figure 6(A) and (B)), Rg remains larger than for WT, but the difference is less. In sharp contrast to polyglutamylation, polyglycylation does not significantly increase the Rg of the α- or β-tubulin tails, irrespective of the length of the modification or its spatial organization (Figure 6(A) and (B), green box bottom row). Hence, we conclude that the observation from the atomistic simulations that polyglutamylation leads to tail expansion and polyglycylation leads to tail collapse is general, and does not depend strongly on the length or spatial organization of the modifications. To visualize this conclusion, Figure 5 shows selected conformations for the β tubulin tails of variants characterized by eight different poly-modification distributions and lengths that illustrate their different effects on Rg.

The high content of negatively charged residues is a functionally important property of tubulin tails (as evident by reports that enzymatic cleavage of tails or increasing salt concentration lead to an increase in the diffusion rate of proteins on MTs).[45,46,48] Since tubulin tails decorate the MT surface, we measured not only the charge content of each variant, but also how modifications affect the

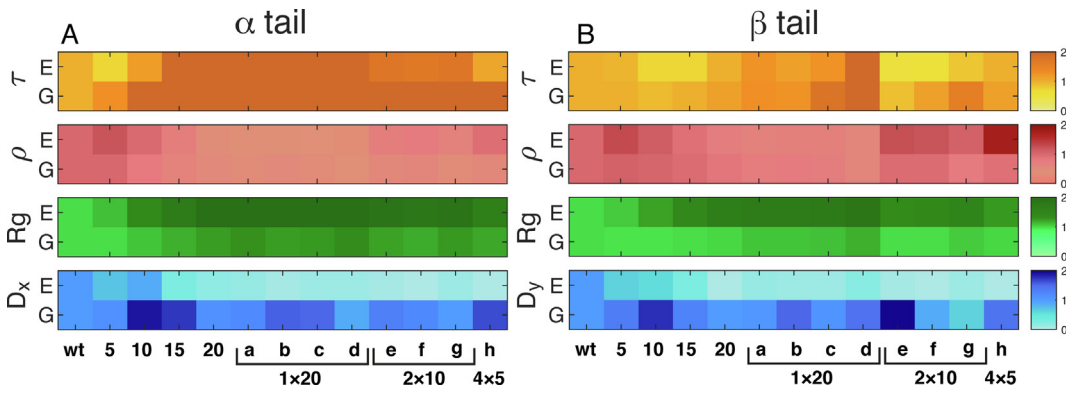

Figure 6. Impact of length and spatial organization of polyglutamylation and polyglycylation on tail structure, function and dynamics. Using the coarse-grained model, we constructed 12 variants in which both the α and β tail were modified with either a polyglutamate or polyglycine substituent chain. We then simulated a WT microtubule and 12 variant microtubules as 3 × 4 tubulin monomer lattices. In the variants bearing polyE5–polyE20 or polyG5–polyG20 chains, the substituent chains were attached at the most common tethering sites on tubulin tails, namely, E435 on the tails of β tubulin and E441 on the tails of α tubulin. In addition, we constructed variants in which the 20-residue modification was tethered as a single substituent chain at one of four different sites, referred to as sites 1–4 (variants a–d). We also constructed three variants in which the addition of 20 residues was achieved by substituting two 10-residue chains that were tethered at sites 1 and 2, 2 and 3, or 3 and 4 (variants e–g). Finally, we constructed one variant in which the addition of 20 residues was achieved by substituting four chains, each 5-residues long, that where tethered at all four tethering sites (variant h). In each panel, we show a different biophysical property of the variant microtubules, normalized by the value for WT microtubules. A value of 1 in each color bar corresponds to the value of unmodified tails and value of 2 corresponds to a property that is twice larger than that of the unmodified tail. Within each panel, the top row shows values for variant microtubules with polyglutamylated tails (E) and the bottom row shows the corresponding values for polyglycylated tails (G). The properties shown are: the diffusion coefficients for the diffusion of EB1 across (D_x, panel A) or along (D_y, panel B) microtubule protofilaments, the radii of tail gyration (Rg), the surface charge coverage of the MT lattice (defined as $\rho = \frac{S_{tail}}{S_{body}} \cdot (number\ of\ charges\ on\ tail)$), and the relaxation times for Rg (τ; see Methods). Panels A and B show data for the tails of α and β tubulin, respectively.

surface charge coverage of the tail-decorated MT lattice, defined as $\rho = \frac{S_{tail}}{S_{body}} \times (no.\ charges)$, where S_{tail} is the projected surface area of a tubulin tail on the MT lattice plane, and S_{body} is the surface area of a tubulin monomer body. Figure 6(A) and (B) (red panels) show that, in the MT lattice context, variants whose tails are substituted with 5–20 glutamates (upper rows, systems 5–20 and a-h) have larger ρ than WT tubulins. The reason is that the increase in the number of charged residues is coupled with an increase in Rg and hence leads to the coverage of a larger fraction of the surface area of the MT lattice with an electronegative "cloud". By contrast, the polyglycine variants show a milder increase in ρ, correlated with the slight increase in Rg (green panels, bottom row). This indicates that the collapse of polyglycine substituent chains onto the tubulin tail results in local screening of the charged residues of tubulin tails, but the surface charge coverage remains similar to WT MTs. By contrast, the expansion of the polyglutamylated tails, leads to surface charge coverage of the MT lattice which is ~ two-fold larger than WT MTs.

Lastly, we examined how the length and spatial organization of modifications affect the dynamics of tubulin tails. In Figure 6(A) and (B) (orange panel), we show the relaxation times (τ) of Rg (see *Methods* for details). The relaxation times of polyglutamylated and polyglycylated α tubulin are ~ 2-fold longer than those of WT tubulin for most substituent chain lengths, anchoring sites, and spatial organizations (Figure 6(A), orange panels, top and bottom rows. The relaxation times of WT α and β tubulin tails are 200 ± 8 and 600 ± 25 ns, respectively). For the tails of α tubulin, MT lattices with short substituent chains (i.e., polyE5 in 5 and in h) are exceptions to the general trend, in that they exhibit a less significant increase in τ compared with that the WT MT lattice. For the tails of β tubulin (Figure 6(B), orange panel), MT lattices 10 and 15 (polyglutamylation only), and e–g (both polyglutamylation and polyglycylation), exhibit shorter Rg relaxation times than WT, and 20 (polyglutamylation only) anchored at various sites (systems a–d) exhibit longer Rg relaxation times than WT. The polyglycylated β tails exhibit longer relaxation times than WT but the effect of polyglycylation is lower than that for the α tails. We conclude: (a) modifications (both polyglutamylation and polyglycylation) slow the dynamics of α-tubulin tails more than β-tubulin tails; and (b) polyglycylation leads to slower dynamics for the tails of both α and β tubulins, whereas polyglutamylation can, in some cases,

lead to faster dynamics. These observations can be explained by the formation of compact conformations by polyglycylation due to the direct interaction of the polyG substituent with the tail which slows down its dynamics. The smaller effect of polyglutamylation of the β tail compared to the α tail can be linked to the original slower relaxation of the β tail that cannot be further decreased by modifications.

Effect of the force field used on conformations of polyglutamylated and polyglycylated tubulin tails

In order to verify that our results are not force-field dependent, we simulated the isolated tails of both α and β tubulin using five different force fields. We examined WT, polyE20-tails, and polyG20-tails using three all-atom explicit solvent force fields: amber99sb-ildn,[49] charmm36m[50] and a99disp.[51] The latter two are force-fields optimized to simulate both folded and unfolded proteins. In addition, we used our calibrated CG model (presented above) and ABSINTH,[52] which is an implicit solvent model that was shown to capture essential features of disordered proteins. Our main motivation is to compare the effect of different force fields on tail conformation (*i.e.*, the degree of compaction/expansion) in polyglycylated and polyglutamated tails.

In Figure 7(A) we show the projection of our simulations on the first two principal components for all the force-fields studied (polyglutamylated tails in orange, polyglycylated tails in cyan). Although the force fields vary in their parameterization and resolution, the configurational space sampled by tubulin tails is similar in all of them, and more limited for polyglycylated tails compared with polyglutamylated tails. In Figure 7(B) we show Rg/Rg_{WT} for α and β tubulin. Our observation that polyglycylated tails (cyan) collapse and polyglutamylated tails (orange) expand is confirmed in all the isolated modified tail simulations. Although the Rg distributions are not identical across force-fields, the general trend that polyglycylated tails collapse and polyglutamylated tails expand is robust. Hence, we conclude that our results are not force-field dependent, and can serve as the basis for predictions in future experimental studies.

Discussion and Conclusions

The genetic and chemical diversity of the electronegative disordered tubulin tails together comprise the so-called "tubulin code", which regulates various aspects of MT function. Extensive efforts to decipher the "tubulin code" have revealed discoveries as to the functional importance of tubulin polyglutamylation and polyglycylation (for detailed reviews about additional PTMs).[6–8,22] However, a quantitative description of the biophysical properties of tubulin tails and their modifications at (near) atomic resolution, which could shed light on the underlying mechanisms by which tubulin PTMs regulate MT function, is lacking. Specifically, understanding of

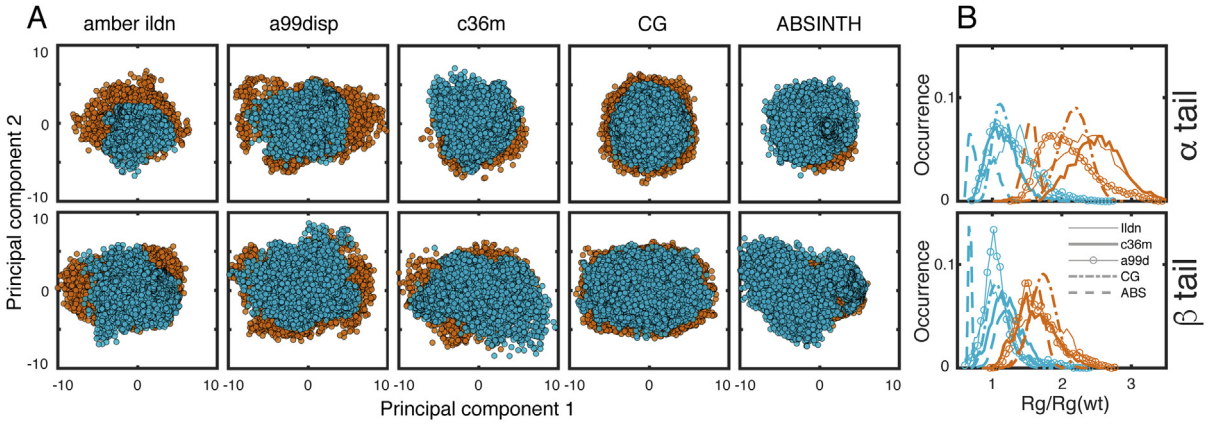

Figure 7. Comparison of the conformational space of polyglutamylated and polyglycylated tails simulated using different force fields. The conformational preferences of the isolated tails (i.e., unattached to a lattice of tubulin bodies) of α tubulin (upper panels) and β tubulin (lower panels) were simulated for WT, polyE20-tails (orange), and polyG20-tails (cyan) using various force-fields. (A) Projection on the first two principal components of five force fields: amber99sb-ildn, charmm36m, a99disp, our CG model, and ABSINTH. Each panel shows the data for a specific force-field, as indicated on the figure, for the tails of α tubulin (upper panels) and β tubulin (lower panels). (B). Distribution of the occurrence of Rg normalized to Rg_{wt} (i.e., Rg/Rg_{wt}) is shown for all five force-fields. Note that for all force fields, the highest-occurrence normalized Rg for polyglycylated tails (cyan) is close to 1, whereas for polyglutamylated tails (orange) the value is close to 2, indicating that for all force fields, the Rg of polyglutamylated tails is ~ 2-fold larger than the Rg of a WT tail, whereas polyglycylation does not affect the dimension of the tails.

how the length, anchoring site, and spatial organization of these specific PTMs affect the biophysical properties of tubulin tails is not known and is therefore the focus of this work.

Here, we used multi-resolution MD simulations to address this task. All-atom MD simulations reveal that tail–body interactions are stronger in a tubulin dimer than in the context of an MT lattice. Therefore, we suggest that previous reports on tail–body interactions based on measurements of tubulin dimers[26,30,31] may not be valid for the case of an MT lattice. In simulations utilizing MT lattices, we found that tail–body interactions are more dominant in α tubulin than in β tubulin, in line with a recent NMR study.[20] Moreover, polyglycylation of α-tubulin tails increases (and polyglutamylation decreases) the tail–body interaction, yet no such effect is detectable when these modifications occur on β-tubulin tails. Hence, it appears that polyglutamylation and polyglycylation of β-tubulin tails do not regulate tail–body interactions. The tails of β tubulin play an exclusive role in regulating the activity of MT-severing enzymes,[12,32] and it was found that the energy barrier for diffusion mediated by β-tubulin tails is higher than the barrier for diffusion mediated by α-tubulin tails.[15] Together, these lines of evidence suggest that the tails of α and β tubulin have two distinct regulatory roles that can be tuned by tubulin PTMs: α-tubulin tails bind to the MT body and regulate MT mechanical stability, whereas β-tubulin tails regulate the interaction with MT-binding proteins.

Next, when simulating tail dynamics in the biologically-relevant context of a 3 × 4 MT lattice, we found that polyglutamylation leads to an expansion of both α and β tubulin tails, whereas polyglycylated tails collapse onto themselves and onto the tubulin tails. The expansion of the polyglutamate substituent chain is expected because of their negative charge. However, although one may also expect the polyglycine substituent chains to increase the Rg of tubulin tails because of excluded volume effects, our results show that polyglycylated tails collapse, suggesting that hydrophobic interactions with additional Gly residues and with the residues of the tail backbone are more dominant than the excluded volume effect. A Flory-type analysis of polyglutamylated tails and polyglycylated tails supports these observations by showing that the value of the Flory exponent ν for polyglycine chain ($\nu \sim 0.6$–0.7) is lower than its value for polyglutamate chain ($\nu \sim 0.9$). It is noteworthy that the value of ν for isolated polyglycynated and polyglutamylated tails are similar to that of the tails in the context of the MT lattice (Figure S4). Hence, although tubulin disordered tails create a molecular brush in the sense that they coat the MT surface, the biophysical properties of the tails are not altered by interactions with neighboring tails. Therefore, they do not resemble the classical form of polymer brushes in which interchain interactions are dominant,[53,54] which was found for example in the case of the disordered protein regions coating the lumen of the nuclear pore complex.[55,56]

Theoretically, many combinations of different PTMs of varying lengths and at different anchoring sites are possible, giving rise to an enormous combinatorial space of the tubulin code. For example, even a single tubulin tail can have a combination of polyglutamate and polyglycine substituent chains at different positions and of different lengths. Using CG-MD, we elucidated the large combinatorial space of the tubulin code, focusing on the addition of 20 polyglutamate and polyglycine residues at different anchoring sites and with different spatial organizations. We found that polyglutamylation leads to expansion of tubulin tails and to a decrease in the diffusion rate of EB1 along and across MT protofilaments, regardless of the precise spatial organization of the poly-modifications. The slower diffusion on polyglutamylated MTs can be attributed not only to the excluded volume induced by the expanded tails, but also to enhanced electrostatic attraction between the diffusing protein and the hyper electronegative glutamylated tubulin tail, as shown previously.[15] Support to our findings arise from the experimental observations that polyglutamylation leads to increased processivity of kinesin-1 and 2 by ~1.5-fold,[11] and to perturbed axonal cargo transport in neurons.[18] In addition, these findings are consistent with a previous study in which we reported that polyglutamylation leads to a decrease in diffusion rate,[15] but we now expand our conclusions to a variety of spatial organizations. Diffusion rate is often anti-correlated with protein affinity for the biopolymer on which it diffuses, since in order for a protein to diffuse and not detach or bind tightly to its substrate, it must bind with intermediate affinity. For diffusion of proteins on DNA and MTs (two negatively charged biopolymers) this fine-tuning is often achieved by the spatial organization of charges on the diffusing protein.[16,57] Since polyglutamylation leads to a decrease in diffusion rate, it is likely that it also leads to an increase in the affinity of proteins for MT in general. Similar suggestions were proposed based on the observation that polyglutamylation acts as a linear affinity tuner of spastin to MTs.[12]

In contrast to polyglutamate substituent chains, polyglycine chains collapse onto themselves and onto the tubulin tail backbone, and therefore do not increase the Rg of either the α- or β-tubulin tails. Moreover, the diffusion rate of EB1 on polyglycylated MT is often faster than the diffusion rate of EB1 on WT MT. It appears that the collapse of polyglycine substituent chains leads to local charge screening of the tubulin tails and therefore, may lead to an increase in diffusion rate, and plausibly to a decrease in the affinity of

proteins for MTs. We note that, although it is tempting to suggest that polyglutamylation leads to an increase in protein affinity for MT and polyglycylation has the opposite effect, our results are not as conclusive for the polyglycylation as for the polyglutamylation of tubulins. It is possible that longer polyglycine substituent chains (substituent chains of up to 40 glycine residues were found in axonemal MTs) may reduce protein affinity for MTs, however these systems were yet to be examined.

The findings reported in this work can be extrapolated to the functional role of polyglutamylation in other proteins.[58] Although polyglutamylation is an uncommon PTM in proteins, it is found also in nucleosome assembly proteins 1 and 2, to which up to nine and 10 glutamates can be added, respectively.[59] The polyglutamylation of nucleosome assembly protein 1 (NAP1) was reported to be vital to its function, and to promote the deposition of a histone protein onto chromatin. Other proteins that undergo polyglutamylation are proline, glutamic acid, and leucine rich protein 1 (PELP1), which is involved in chromatin remodeling and also binds histones.[60] In light of our findings, it is possible that the addition of negatively charged polyglutamate substituent chains to NAP1/2 or PELP1 increases their affinity for the positively charged histone protein, and thereby enables more efficient deposition of histone onto chromatin.[61]

To conclude, this work provides a detailed molecular quantification of the biophysical properties of tubulin tails and their poly-modifications in the context of an MT lattice, which is a biologically crucial form of tubulin in the cell. The molecular brush properties of MT are affected differently by modifying the disordered tails with poly-glutamylation or poly-glycylation, which consequently may alter the affinity of MT-binding proteins to MT as well as the mechanical stability of the MT. While the modifications often affect similarly both α- and β-tails, their response to the modifications can deviate, thus suggesting another layer of complexity of the "tubulin code". Our results explain existing experimental results, and provide predictions regarding the impact of the length and spatial distribution of tubulin poly-modifications on tubulin tail biophysics and interactions with other proteins.

Methods

Model generation

To study the conformational dynamics of tubulin tails in the context of an MT lattice, we constructed an MT lattice consisting of three protofilaments each consisting of two heterodimeric tubulin molecules (*i.e.*, the lattice consists of 3 × 4 monomeric tubulin proteins organized as 3 × 2 tubulin heterodimers). The coordinates of the MT lattice were based on the structure of a single isoform neuronal human MT (PDB ID 5JCO).[62] The disordered tails (residues 438–451 of α tubulin and 427–450 of β tubulin) were added as linear chains to the C-terminal of each tubulin monomer. A more realistic conformation of the tails was obtained from the simulations (see below).

In this work, we chose to study MTs bearing the tails of isoform α1A and β3, which comprise 14 and 24 residues, respectively. The sequences of the tubulin tails are DSVEGEGEEEGEEY for α tubulin (isoform α1A, net charge of −8) and DATAEEEGEMYEDDEEESEAQGPK for β tubulin (isoform β3, net charge of −11). The underlined Glu served as the PTM site, unless stated otherwise.

Modeling post-translational modifications

The effect of polyglutamylation or polyglycylation on the biophysical properties of tubulin tails was studied by modifying the tails through the tethering of polyglutamic acids or polyglycine substituent chains, respectively. The substituent chains were added by creating a peptide bond between the amino terminal of the chains and the C_γ atom of glutamate 445 in α tubulin or glutamate 435 in β tubulin. These sites were previously identified as common positions for polyglutamylation[40–42] and were used as modification sites to study the effect of polyglutamylation on the activity of motor proteins.[11] We constructed a model of a MT comprising a 3 × 4 monomeric tubulin lattice in which substituent chains of length 0 (WT), 5, 10, 15, and 20 residues are anchored to the tails of α and β tubulins at positions E445 and E435, respectively. We refer to these MT lattices as WT, 5, 10, 15, and 20, respectively. These variants were studied with both atomistic and CG models.

In our CG model (see below), we constructed additional variants using various attachment positions for the substituent chains. In addition to the E435 attachment site, glutamates 438, 440, and 441 have also been identified experimentally as potential modification sites on the β tail[40,43] and were therefore explored in this study. Similarly, three additional glutamates, namely E441, E447, and E450, were selected as additional modifications sites on the α tails. Glutamates 441 and 447 were reported to be modifications sites in previous studies, and E450 was chosen because it is the glutamate furthest from the last documented modification site.[41,44] These eight selected sites on the tails of α and β tubulin can yield many combinations of modifications. In our study, we concentrate on several options of pairs with coupling between the modifications in α and β tubulin tails. Accordingly, modifications at E441, E445, E447, or E450 on an α tubulin tail were coupled with modifications at E435, E438, E440, or E441 on a β tubulin tail,

respectively. For convenience, we label the pairings of positions on α and β tails using indices: site 1 refers to α441 paired with β435; site 2 refers to α445 paired with β438; site 3 refers to α447 paired with β440; and site 4 refers to α450 paired with β441.

In this manner, we constructed a model WT tubulin and 12 variants, each substituted with 20 glutamate or 20 glycine residues. In four variants, a single 20-residue substituent chain was attached to each of the α and β tubulin tails at site 1, 2, 3 or 4 (Figure 5, top row, variants a–d). In three other variants, two chains, each 10 residues long, were attached, each at a different tail position: sites 1 and 2, 2 and 3, or 3 and 4 (Figure 5, middle row, variants e–g). These three variants were chosen among six possibilities as they capture placing the two chains at both ends of the tails as well as in the center. Finally, we constructed a variant in which the 20 modification residues were distributed between four chains each of length five residues that were attached at each of the selected attachment sites on the tails (Figure 5, bottom row, variant h). In total, eight variants of modified α and β tails substituted with 20 residues were designed. These variants were utilized to construct both polyglutamylated and polyglycylated microtubules modelled as a 3 × 4 monomeric tubulin lattices. In total, one WT, 12 polyglutamylated and 12 polyglycylated MT lattices were studied.

All- atom simulations

The conformational dynamics of tubulin tails and their modifications were studied using all-atom molecular dynamics simulations. The simulations were performed using GROMACS[63] version 2018.3. The molecular system was solvated in a box with periodic boundary conditions containing pre-equilibrated SPC/E water molecules. Na^+ and Cl^- ions were added to maintain overall system neutrality with salt concentration of 0.125 mM. We used the AMBER99SB-ILDN[49] force field. The LINCS algorithm[64] was used to control bonds during the simulation. The leapfrog algorithm was employed with steps of 2 fs.

In order to enhance the conformational sampling of the disordered tubulin tails, we first simulated the system at 400 K for 10 ns, and used conformations from the high temperature run as initial conformations for simulations at more realistic temperatures. Hence, the temperature was controlled at 400 K using a modified scheme of the Berendsen thermostat.[65] The system was minimized using the steepest descent algorithm. Next, the system was equilibrated under an NVT ensemble and an NPT ensemble (100 ps each phase). Production runs were executed at constant pressure (1 atm) for 10 ns. During production runs, the Cα atoms of the MT body residues were kept fixed to prevent lattice distortion and to enhance computation performance.

Selected conformations from the simulations at 400 K were used as starting points for at least seven independent simulations at 300 K. Each initial conformation was re-equilibrated using the same procedure described for the 400 K simulations. Production runs were executed for 100 ns on the PizDaint supercomputer at the Swiss National Center for Computing. The Cα atoms of the MT body were kept fixed during the simulations. Avoiding internal flexibility for the MT-body is a reasonable assumption given the rigidity of MT structures. This approach also avoids deformation of the MT slice used in our simulations. Furthermore, the internal dynamics of the tubulin monomers is not expected to contribute to tail dynamics or to protein diffusion on MT. Atomistic simulations of MT lattices were performed for WT MT, and MT with 5, 10, 15 or 20 added Glu or Gly residues, for a total of nine systems. The lattices comprised of polyE20 (or polyG20) comprise 2,442,109 (2,442,745) atoms, respectively (including water and salt). In total, the accumulated simulation time for the lattices was 7.8 μs.

Force field validation

In order to test the sensitivity of the results on the force-field applied, we studied the conformational dynamics of peptides of α and β tubulin tails using additional force-fields for WT-tails and for polyE20-tails or polyG20-tails. Hence, for each force-field we simulated six different variants. For this set of simulations we used the all atom AMBER99SB-ILDN,[49] charmm36m[50] and a99disp[51] force fields. The two latter force-fields were optimized to improve accuracy in the simulation of proteins that have ordered and disordered regions. In addition, we used the implicit solvent model ABSINTH,[52] and our CG model (described below). For the all-atom models, the peptides were solvated, their energy was minimized, and they were equilibrated at 300 K as described above. Production runs were executed for 1000 ns per peptide, yielding 18 μs in total.

For the ABSINTH force field, the peptides were first simulated using Monte-Carlo simulations for 300,000 steps in order to obtain a realistic configuration without steric clashes. The end conformation of the Monte-Carlo simulations was used as the initial structure for MD simulations, in which we used 4 fs time steps for 1000 ns at 300 K. In the CG model, we ran 10 simulation repeats at a temperature of T = 0.4 for 10^7 steps.

Coarse-grained molecular dynamics simulations

The dynamics of tubulin tails was studied also using CG-MD simulations that enable the

investigation of many variant systems at a relatively low computational cost, and also enable the sampling of long time-scale process, such as diffusion of proteins on MT. In this model, each residue was represented by a single bead at the position of its Cα atom.

The force-field applied in our simulations used a native-topology based model that includes a Lennard-Jones potential to reward native contacts and a repulsive potential to penalize non-native contacts.[66–68] Electrostatic interactions between charged residues were modeled using the Debye-Hückel potential.[69] The explicit form of the force field is:

$$V(\Gamma,\Gamma_0)=\sum_{bonds}K_{bonds}\left(b_{ij}-b_{ij}^0\right)+\sum_{angles}K_{angles}\left(\theta_{ijk}-\theta_{ijk}^0\right)+\sum_{dihedrals}K_{dihedrals}\left(\left[1-\cos\left(\varphi_{ijkl}-\varphi_{ijkl}^0\right)\right]+\frac{1}{2}[1-\cos(3(\varphi_{ijkl}-\varphi_{ijkl}^0))]\right)+\sum_{i\neq j}K_{contacts}[5\left(\frac{A_{ij}}{r_{ij}}\right)^{12}-6\left(\frac{A_{ij}}{r_{ij}}\right)^{10}]+\sum_{i\neq j}K_{repulsions}\left(\frac{C_{ij}}{r_{ij}}\right)^{12}+\sum_{i\neq j}K_{electrostatics}B(\kappa)q_iq_j\frac{e^{-\kappa r}}{\varepsilon_r r_{ij}}$$

where K_{bonds} = 100 kcal mol^{-1} Å^{-2}, K_{angles} = 20 kcal mol^{-1}, and $K_{dihedrals}$, $K_{contacts}$, $K_{repulsion}$ are each valued at 1 kcal mol^{-1}. The term b_{ij} is the distance (in Å) between bonded beads *i-j*, θ_{ijk} is the angle (in radians) between sequentially bonded beads *i-j-k*, φ_{ijkl} is the dihedral angle (in radians) between sequentially bonded backbone beads *i-j-k-l*, and r_{ij} is the distance (in Å) between beads *i-j* in a given conformation along the trajectory. A_{ij} is the distance (in Å) between beads *i-j* that are in contact with each other in the experimentally determined structure. The parameters denoted with the superscript 0 (x^0) represent the minima of the various potential energy terms, and were assigned according to the atomic coordinates of the structures. C_{ij} is the sum of radii for any two beads not forming a native contact; the repulsion radius of the backbone bead is 2.0 Å. The last term in the force field is the Debye-Hückel potential, where $K_{electrostatics}$ = 332 kcal Å mol^{-1} e^{-2}, $q_{i/j}$ is the sign of the charged residue, ε_r is the dielectric constant, κ is the screening factor, B(κ) is the salt-dependent coefficient, and r_{ij} is the distance (in Å) between charged residues *i* and *j*. We note that, because of the coarse-grained representation of the systems, the effective salt concentration may correspond to a value higher (by a factor of ~ 3) than for an atomistic representation. More details regarding the Debye-Hückel potential can be found in Ref.[69]

As in the all-atom simulations, the beads of the structured part of the MT were kept fixed in our simulations whereas the MT-tails were flexible. The flexibility of the disordered MT-tails was controlled by their bond and dihedral angles. The dynamics of tubulin tails was simulated using the Langevin equation. The simulation temperature was set to 0.4 (reduced units). The dielectric constant was 80, and the salt concentration was 0.06 M.

To reduce computational time, electrostatic interactions between the tubulin tails and the charged residues of both α and β tubulins located at the interior of the microtubules were eliminated. This elimination did not affect the properties of the MT surface, which is the side relevant to the diffusion process and tail–body interactions, as the distance between the MT lumen and surface is ~ 40 Å.

Calibration of the coarse-grained polyglycylated variants

For the polyglycylated tails, hydrophobic interactions were included based on the hydrophobicity scale model (HPS)[39]. In this model, a hydrophobicity scale λ is assigned to each residue, such that the most hydrophobic residue (Trp) has a value of λ = 1 and the least hydrophobic residue (Arg) has a value of λ = 0. The interaction between two residues i-j is defined by a scaled Lennard-Jones term:

$$\phi_{HPS}(r)=w*\lambda_{ij}[5\left(\frac{\sigma_{ij}}{r_{ij}}\right)^{12}-6\left(\frac{\sigma_{ij}}{r_{ij}}\right)^{10}]$$

where λ_{ij} is the arithmetic mean hydrophobicity scale of two interacting residues ($\lambda_{ij}=(\lambda_i+\lambda_j)/2$) and σ_{ij} is the amino acid size ($\sigma_{ij}=(\sigma_i+\sigma_j)/2$). The values of λ and σ were taken from Ref.[39] Based on the results from our atomistic simulations, which showed that polyglycine residues interact mainly with themselves or the tail residues (Figure 3(A) and (B)), only intra-tail hydrophobic interactions were included in our model. The term *w* is a calibration parameter, which is tuned such that the Rg of polyglycylated tails matches the Rg obtained from atomistic simulations (Figure S2-3).

To calibrate our CG model, we first scanned salt concentrations to find the conditions at which the Rg of polyE5–polyE20 correlated linearly with a slope of ~ 1 with the atomistic simulations. We found this value to be a salt concentration of 60 mM. Next, we scanned values of w to obtain a linear correlation between the CG and atomistic simulations of polyglycylated tails. The optimal value for *w* was found to be 0.275.

Calculation of Flory exponents

Rg as a function of the inter-residue sequence separation |i-j|, was calculated for WT or modified tubulin tails (see main text for details). For each fixed sequence separation |i-j|, Rg was averaged over all possible combinations using a sliding window with size |i-j|, with the origin of the window ranging from 0 to N-|i-j|, with N being the total number of residues in the relevant polypeptide. Data were then fit to the Flory scaling expression: $Rg \sim |i-j|^{\nu}$.

Diffusion of EB1 on MT

To study the diffusion of EB1 (residues 1–130,[70] pdb ID 1PA7) along MTs, we constructed an MT lattice as described above, but we used a larger lattice that consists of four protofilaments, each consisting of three heterodimeric tubulin molecules (*i.e.*, the lattice consisted of 6 × 4 monomeric tubulin proteins). EB1 and MT were confined in a box of dimensions 350 × 400 × 330 Å, and the longitudinal direction of the MT was aligned along the Y-axis. We preformed 50 simulations consisting of 2×10^7 essential MD steps to achieve sufficient sampling. Trajectory frames were saved every 1000 steps. Periodic boundary conditions were not used in this model.

Calculation of diffusion coefficients

The trajectories from the CG simulations were analyzed using in-house scripts. The mean square displacements (MSD) of the proteins' centers of mass (COM) were calculated using the equation:

$$MSD(\tau) = \sum_{i=t_0}^{t-\tau} \frac{(r_{i+\tau} - r_i)^2}{t-\tau} = 2dD\tau$$

where r is the position of the protein COM, t is the number of time steps measured, and τ is the measurement window ranging from t_0 to t. The slope of the MSD is $2dD$, where d is the dimensionality of diffusion and D is the diffusion coefficient, which was calculated between time frames 1500 and 3000 for diffusion on MTs, because shorter time scales do not capture the slow diffusion process.

Relaxation times

In order to derive relaxation times for Rg, the correlation function of Rg was calculated by:

$$C(\tau) = \sum_{t=1}^{t_{max}-\tau} \frac{(Rg(t) - < Rg >) \cdot (Rg(t+\tau) - < Rg >)}{(Rg(t) - < Rg >)^2}$$

where τ is the time lag for the correlation function and < Rg > is the mean value of Rg. C(τ) was fitted to a single exponential decaying function:

$$C(\tau) = ae^{-\frac{\tau}{\tau}}$$

where the time constant τ was defined as the relaxation time of the Rg correlation function.

Author contribution

LSB and YL designed the research and wrote the manuscript. LSB performed the research and analyzed the data.

CRediT authorship contribution statement

Lavi S. Bigman: Conceptualization, Formal analysis, Visualization. **Yaakov Levy:** Conceptualization, Visualization.

Acknowledgements

We thank Harry Mark Greenblatt for assistance with the atomistic model of tubulin PTMs, and the Swiss national computing center (project number S918) for GPU time. Y. L. holds The Morton and Gladys Pickman professional chair in Structural Biology.

Declaration of Competing Interest

The authors declare that they have no known competing financial interests or personal relationships that could have appeared to influence the work reported in this paper.

Appendix A. Supplementary material

Supplementary data to this article can be found online at https://doi.org/10.1016/j.jmb.2021.166988.

Received 23 February 2021;
Accepted 7 April 2021;
Available online 16 April 2021

Keywords:
intrinsically disordered proteins;
microtubule;
post-translational modifications;
tubulin code;
diffusion

References

1. Nogales, E., Kellogg, E.H., (2017). Challenges and opportunities in the high-resolution cryo-EM visualization of microtubules and their binding partners. *Curr. Opin. Struct. Biol.*, **46**, 65–70.
2. Li, H., DeRosier, D.J., Nicholson, W.V., Nogales, E., Downing, K.H., (2002). Microtubule Structure at 8 Å Resolution. *Structure*, **10**, 1317–1328.
3. Roll-Mecak, A., (2015). Intrinsically disordered tubulin tails: Complex tuners of microtubule functions?. *Semin. Cell Dev. Biol.*, **37**, 11–19.
4. Wehenkel, A., Janke, C., (2014). Towards elucidating the tubulin code. *Nature Cell Biol.*, **16**, 303–305.
5. Yu, I., Garnham, C.P., Roll-Mecak, A., (2015). Writing and Reading the Tubulin Code. *J. Biol. Chem.*, **290**, 17163–17172.

6. Janke, C., Magiera, M.M., (2020). The tubulin code and its role in controlling microtubule properties and functions. *Nature Rev. Mol. Cell Biol.*, **1–20**
7. Roll-Mecak, A., (2020). The Tubulin Code in Microtubule Dynamics and Information Encoding. *Dev. Cell.*, **54**, 7–20.
8. Roll-Mecak, A., (2019). How cells exploit tubulin diversity to build functional cellular microtubule mosaics. *Curr. Opin. Cell Biol.*, **56**, 102–108.
9. Wang, Z., Sheetz, M.P., (2000). The C-Terminus of Tubulin Increases Cytoplasmic Dynein and Kinesin Processivity. *Biophys. J.*, **78**, 1955–1964.
10. Marya, P.K., Syed, Z., Fraylich, P.E., Eagles, P.A., (1994). Kinesin and tau bind to distinct sites on microtubules. *J. Cell Sci.*, **107**, 339–344.
11. Sirajuddin, M., Rice, L.M., Vale, R.D., (2014). Regulation of microtubule motors by tubulin isotypes and post-translational modifications. *Nature Cell Biol.*, **16**, 335–344.
12. Valenstein, M.L., Roll-Mecak, A., (2016). Graded Control of Microtubule Severing by Tubulin Glutamylation. *Cell.*, **164**, 911–921.
13. Shin, S.C., Im, S.K., Jang, E.H., Jin, K.S., Hur, E.M., Kim, E.E.K., (2019). Structural and Molecular Basis for Katanin-Mediated Severing of Glutamylated Microtubules. *Cell Rep.*, **26**, 1357–1367.e5.
14. Sandate, C.R., Szyk, A., Zehr, E.A., Lander, G.C., Roll-Mecak, A., (2019). An allosteric network in spastin couples multiple activities required for microtubule severing. *Nature Struct. Mol. Biol.*, **26**, 671–678.
15. Bigman, L.S., Levy, Y., (2020). Tubulin tails and their modifications regulate protein diffusion on microtubules. *Proc. Natl. Acad. Sci. USA*, **117**, 8876–8883.
16. Bigman, L.S., Levy, Y., (2020). Protein Diffusion on Charged Biopolymers: DNA versus Microtubule. *Biophys. J.*, **118**, 3008–3018.
17. Cooper, J.R., Wordeman, L., (2009). The diffusive interaction of microtubule binding proteins. *Curr. Opin. Cell Biol.*, **21**, 68–73.
18. Magiera, M.M., Bodakuntla, S., Žiak, J., Lacomme, S., Marques Sousa, P., Leboucher, S., Hausrat, T.J., Bosc, C., et al., (2018). Excessive tubulin polyglutamylation causes neurodegeneration and perturbs neuronal transport. *EMBO J.*, e100440.
19. Magiera, M.M., Janke, C., (2014). Posttranslational modifications of Tubulin. *Curr. Biol.*, **24** (9), R351–R354.
20. Wall, K.P., Hart, H., Lee, T., Page, C., Hawkins, T.L., Hough, L.E., (2020). C-Terminal Tail Polyglycylation and Polyglutamylation Alter Microtubule Mechanical Properties. *Biophys. J.*, **118**, 597a.
21. Gadadhar, S., Alvarez Viar, G., Hansen, J.N., Gong, A., Kostarev, A., Ialy-Radio, C., Leboucher, S., Whitfield, M., et al., (2021). Tubulin glycylation controls axonemal dynein activity, flagellar beat, and male fertility. *Science (80-)*, **371**, eabd4914.
22. Magiera, M.M., Singh, P., Gadadhar, S., Janke, C., (2018). Tubulin Posttranslational Modifications and Emerging Links to Human Disease. *Cell*, **173**, 1323–1327.
23. Redeker, V., (2010). Mass spectrometry analysis of C-terminal posttranslational modifications of tubulins. Academic Press Inc..
24. Geimer, S., Teltenkötter, A., Plessmann, U., Weber, K., Lechtreck, K.F., (1997). Purification and characterization of basal apparatuses from a flagellate green alga. *Cell Motil. Cytoskeleton.*, **37**, 72–85.
25. Redeker, V., Levilliers, N., Schmitter, J.M., Le Caer, J.P., Rossier, J., Adoutte, A., Bré, M.H., (1994). Polyglycylation of tubulin: A posttranslational modification in axonemal microtubules. *Science (80-)*, **266**, 1688–1691.
26. Wall, K.P., Pagratis, M., Armstrong, G., Balsbaugh, J.L., Verbeke, E., Pearson, C.G., Hough, L.E., (2016). Molecular determinants of tubulin's C-terminal tail conformational ensemble. *ACS Chem. Biol.*, **11**, 2981–2990.
27. Mahalingan, K.K., Keith Keenan, E., Strickland, M., Li, Y., Liu, Y., Ball, H.L., Tanner, M.E., Tjandra, N., Roll-Mecak, A., (2020). Structural basis for polyglutamate chain initiation and elongation by TTLL family enzymes. *Nature Struct. Mol. Biol.*, **27**, 802–813.
28. Rogowski, K., Juge, F., van Dijk, J., Wloga, D., Strub, J.-M., Levilliers, N., Thomas, D., Bré, M.-H., et al., (2009). Evolutionary Divergence of Enzymatic Mechanisms for Posttranslational Polyglycylation. *Cell*, **137**, 1076–1087.
29. van Dijk, J., Rogowski, K., Miro, J., Lacroix, B., Eddé, B., Janke, C., (2007). A Targeted Multienzyme Mechanism for Selective Microtubule Polyglutamylation. *Mol. Cell.*, **26**, 437–448.
30. Laurin, Y., Eyer, J., Robert, C.H., Prevost, C., Sacquin-Mora, S., (2017). Mobility and Core-Protein Binding Patterns of Disordered C-Terminal Tails in β-Tubulin Isotypes. *Biochemistry*, **56**, 1746–1756.
31. Freedman, H., Luchko, T., Luduena, R.F., Tuszynski, J.A., (2011). Molecular dynamics modeling of tubulin C-terminal tail interactions with the microtubule surface. *Proteins Struct. Funct. Bioinforma.*, **79**, 2968–2982.
32. Zehr, E.A., Szyk, A., Szczesna, E., Roll-Mecak, A., (2020). Katanin Grips the β-Tubulin Tail through an Electropositive Double Spiral to Sever Microtubules. *Dev. Cell.*, **52**, 118–131.e6.
33. Flory, P.J., (1953). *Principles of Polymer Chemistry*,, **10** Cornell Univ. Press, Ithaca, NY London, UK.
34. Vitalis, A., Wang, X., Pappu, R.V., (2007). Quantitative characterization of intrinsic disorder in polyglutamine: Insights from analysis based on polymer theories. *Biophys. J.*, **93**, 1923–1937.
35. Hofmann, H., Soranno, A., Borgia, A., Gast, K., Nettels, D., Schuler, B., (2012). Polymer scaling laws of unfolded and intrinsically disordered proteins quantified with single-molecule spectroscopy. *Proc. Natl. Acad. Sci.*, **109**, 16155–16160.
36. Tran, H.T., Mao, A., Pappu, R.V., (2008). Role of backbone-solvent interactions in determining conformational equilibria of intrinsically disordered proteins. *J. Am. Chem. Soc.*, **130**, 7380–7392.
37. de Gennes, P.G., Pincus, P., Velasco, R.M., Brochard, F., (1976). Remarks on polyelectrolyte conformation To cite this version. *J. Phys.*, **37**, 1461–1473.
38. Ha, B., Thirumalai, D., (1992). Conformations of a polyelectrolyte chain. *Phys. Rev. A.*, **46**, 3012–3015.
39. Dignon, G., Zheng, W., Kim, Y., Best, R., Mittal, J., (2018). Sequence determinants of protein phase behavior from a coarse-grained model. *PLoS Comput. Biol.*, **14**, 238170
40. Rüdiger, M., Plessman, U., Klöppel, K.-D., Wehland, J., Weber, K., (1992). Class II tubulin, the major brain β tubulin isotype is polyglutamylated on glutamic acid residue 435. *FEBS Letters*, **308**, 101–105.
41. Eddé, B., Rossier, J., Le Caer, J.P., Desbruyères, E., Gros, F., Denoulet, P., (1990). Posttranslational glutamylation of alpha-tubulin. *Science*, **247**, 83–85.

42. Westermann, S., Weber, K., (2003). Post-translational modifications regulate microtubule function. *Nature Rev. Mol. Cell Biol.*, **4**, 938–947.
43. Rüdiger, M., Plessmann, U., Rüdiger, A.H., Weber, K., (1995). Β Tubulin of Bull Sperm Is Polyglycylated. *FEBS Letters*, **364**, 147–151.
44. Sahab, Z.J., Kirilyuk, A., Zhang, L., Khamis, Z.I., Pompach, P., Sung, Y., Byers, S.W., (2012). Analysis of tubulin alpha-1A/1B C-terminal tail post-translational poly-glutamylation reveals novel modification sites. *J. Proteome Res.*, **11**, 1913–1923.
45. Helenius, J., Brouhard, G., Kalaidzidis, Y., Diez, S., Howard, J., (2006). The depolymerizing kinesin MCAK uses lattice diffusion to rapidly target microtubule ends. *Nature*, **441**, 115–119.
46. Forth, S., Hsia, K.C., Shimamoto, Y., Kapoor, T.M., (2014). Asymmetric friction of nonmotor MAPs can lead to their directional motion in active microtubule networks. *Cell*, **157**, 420–432.
47. Brouhard, G.J., Stear, J.H., Noetzel, T.L., Al-Bassam, J., Kinoshita, K., Harrison, S.C., Howard, J., Hyman, A.A., (2008). XMAP215 Is a Processive Microtubule Polymerase. *Cell*, **132**, 79–88.
48. Hinrichs, M.H., Jalal, A., Brenner, B., Mandelkow, E., Kumar, S., Scholz, T., (2012). Tau protein diffuses along the microtubule lattice. *J. Biol. Chem.*, **287**, 38559–38568.
49. Lindorff-Larsen, K., Piana, S., Palmo, K., Maragakis, P., Klepeis, J.L., Dror, R.O., Shaw, D.E., (2010). Improved side-chain torsion potentials for the Amber ff99SB protein force field. *Proteins Struct. Funct. Bioinforma.*, **78**, 1950–1958.
50. Huang, J., Rauscher, S., Nawrocki, G., Ran, T., Feig, M., De Groot, B.L., Grubmüller, H., MacKerell, A.D., (2016). CHARMM36m: An improved force field for folded and intrinsically disordered proteins. *Nature Methods*, **14**, 71–73.
51. Robustelli, P., Piana, S., Shaw, D.E., (2018). Developing a molecular dynamics force field for both folded and disordered protein states. *Proc. Natl. Acad. Sci. USA*, **115**, E4758–E4766.
52. Vitalis, A., Pappu, R.V., (2012). ABSINTH: A new continuum solvation model for simulations of polypeptides in aqueous solutions. *J. Comput. Chem.*, **32**, 174–182.
53. Netz, R.R., Andelman, D., (2003). Neutral and charged polymers at interfaces. *Phys. Rep.*, **380**, 1–95.
54. Rubinstein, M., Colby, R.H., (2003). Polymer physics. *Polym. Int.*, **440**
55. Raveh, B., Karp, J.M., Sparks, S., Dutta, K., Rout, M.P., Sali, A., Cowburn, D., (2016). Slide-and-exchange mechanism for rapid and selective transport through the nuclear pore complex. *Proc. Natl. Acad. Sci. USA*, **113**, E2489–E2497.
56. Lim, R.Y.H., Fahrenkrog, B., Köser, J., Schwarz-Herion, K., Deng, J., Aebi, U., (2007). Nanomechanical basis of selective gating by the nuclear pore complex. *Science (80-)*, **318**, 640–643.
57. Zandarashvili, L., Esadze, A., Vuzman, D., Kemme, C.A., Levy, Y., Iwahara, J., (2015). Balancing between affinity and speed in target DNA search by zinc-finger proteins via modulation of dynamic conformational ensemble. *Proc. Natl. Acad. Sci. USA*, **112**, E5142–E5149.
58. Ludueña, R.F., (2013). A Hypothesis on the Origin and Evolution of Tubulin. *Int. Rev. Cell Mol. Biol.*,, 41–185.
59. Regnard, C., Desbruyères, E., Huet, J.C., Beauvallet, C., Pernollet, J.C., Eddé, B., (2000). Polyglutamylation of nucleosome assembly proteins. *J. Biol. Chem.*, **275**, 15969–15976.
60. Kashiwaya, K., Nakagawa, H., Hosokawa, M., Mochizuki, Y., Ueda, K., Piao, L., Chung, S., Hamamoto, R., et al., (2010). Involvement of the tubulin tyrosine ligase-like family member 4 polyglutamylase in PELP1 polyglutamylation and chromatin remodeling in pancreatic cancer cells. *Cancer Res.*, **70**, 4024–4033.
61. Miller, K.E., Heald, R., (2015). Glutamylation of Nap1 modulates histone H1 dynamics and chromosome condensation in Xenopus. *J. Cell Biol.*, **209**, 211–220.
62. Vemu, A., Atherton, J., Spector, J.O., Szyk, A., Moores, C. A., Roll-Mecak, A., (2016). Structure and dynamics of single-isoform recombinant neuronal human tubulin. *J. Biol. Chem.*, **291**, 12907–12915.
63. Pronk, S., Páll, S., Schulz, R., Larsson, P., Bjelkmar, P., Apostolov, R., Shirts, M.R., Smith, J.C., et al., (2013). GROMACS 4.5: A high-throughput and highly parallel open source molecular simulation toolkit. *Bioinformatics*, **29**, 845–854.
64. Hess, B., Bekker, H., Berendsen, H.J.C., Fraaije, J.G.E.M., (1997). LINCS: A Linear Constraint Solver for molecular simulations. *J. Comput. Chem.*, **18**, 1463–1472.
65. Bussi, G., Donadio, D., Parrinello, M., (2007). Canonical sampling through velocity rescaling. *J. Chem. Phys.*, **126**, 014101
66. Clementi, C., Nymeyer, H., Onuchic, J.N., (2000). Topological and energetic factors: What determines the structural details of the transition state ensemble and "en-route" intermediates for protein folding? An investigation for small globular proteins. *J. Mol. Biol.*, **298**, 937–953.
67. Noel, J.K., Whitford, P.C., Sanbonmatsu, K.Y., Onuchic, J. N., (2010). SMOG@ctbp: Simplified deployment of structure-based models in GROMACS. *Nucleic Acids Res.*, **38**, W657–W661.
68. Noel, J.K., Levi, M., Raghunathan, M., Lammert, H., Hayes, R.L., Onuchic, J.N., Whitford, P.C., (2016). SMOG 2: A Versatile Software Package for Generating Structure-Based Models. *PLoS Comput. Biol.*, **12**, e1004794
69. Azia, A., Levy, Y., (2009). Nonnative electrostatic interactions can modulate protein folding: molecular dynamics with a grain of salt. *J. Mol. Biol.*, **393**, 527–542.
70. Hayashi, I., Ikura, M., (2003). Crystal structure of the amino-terminal microtubule-binding domain of end-binding protein 1 (EB1). *J. Biol. Chem.*, **278**, 36430–36434.